Phil. Trans. R. Soc. Lond. A **308**, 427–444 (1983)
Printed in Great Britain

Observations on the energy balance of internal waves during JASIN

By M. G. Briscoe
Woods Hole Oceanographic Institution, Woods Hole, Massachusetts 02543, *U.S.A.*

Depth-integrated horizontal kinetic energy (HKE) in the frequency band 0.1–4 cycles per hour is used to estimate the time variation at one site of internal wave energy over a 40 day period during JASIN 1978. The HKE smoothed over three days varies from 400 to 1500 J m^{-2}. The canonical Garrett–Munk total energy of 3800 J m^{-2} would provide about 1400 J m^{-2} of HKE in this high frequency band; a scaled-down estimate based on local mean buoyancy frequency and water depth suggests 450 J m^{-2}.

The first part of the record (1 to about 16 August) slowly grows then decays in energy to the record minimum at rates between 0.6 and -1 mW m^{-2}, followed by about 11 days of sporadic growth and decay at rates between 3 and -0.8 mW m^{-2} to the record maximum, and then a week of fast decay at rates between -2 and -1 mW m^{-2}.

A speculative balance of possible energy sources, sinks, and advection/propagation is discussed. The tentative conclusion is that horizontal shears and wind stress fluctuations are the principal energy sources, the latter possibly via interacting surface waves, and that loss of energy from the internal wave continuum to the near-inertial band may be a major sink of HKE. A surprising heuristic correspondence is shown between the amplitude of the local surface wavefield, and the internal wave energy 11 days later.

Introduction

In 1893, during his passage from Oslo across the Barents and Kara seas on the way to not quite getting to the North Pole, Fridtjof Nansen observed a reduction in the forward motion of the *Fram* while sailing on a thin layer of fresh water overlying heavier salty water. A few years later Walfrid Ekman published an explanation of this 'dead water' in terms of the ship's momentum being lost to the momentum of internal waves being generated on the interface between the fresh and salty water. This was a clear case of internal wave generation from an unambiguous source.

Since then, the identification of internal wave sources and sinks in the observational record has seen little progress, except notably for wind-generated near-inertial motions (see for example Weller 1982). Theoretical estimation of the efficiency of various sources and sinks has, on the other hand, been a popular pastime. Thorpe (1975) has reviewed the status of generation and dissipation theory, McComas & Müller (1981) consider the balance of dynamical processes, and Olbers (1983) has discussed energy balances in the context of appropriate models for the internal wavefield. See also Bell (1975, 1978), Garrett (1979), Käse (1979), (Käse & Olbers (1979), Leaman (1976), Müller *et al.* (1978), and Ruddick (1980).

Gregg & Briscoe (1979) point out the importance of knowing the energy balance in assessing the role of internal waves in mixing the ocean or as part of a chain of energy flow from, say, eddies into small-scale dissipation; see their figure 1. The focus of this paper is to try from observations to choose between the two kinds of balances they discuss in that figure: does a lot of energy pass through the internal wavefield, or only a little?

An anthropomorphic view of the internal wavefield would suggest that its purpose is to convert (via nonlinear wave–wave interactions) low frequency, large-vertical-scale, nearly *horizontal*

motions into high frequency, small-vertical-scale, nearly *vertical* motions that can therefore work against gravity and thereby dissipate energy. The internal wave dynamics also spread locally generated motions vertically into the volume and horizontally into other areas (Fu 1981). Thus a local wind storm may have surface stresses that result in near-inertial internal waves that propagate far away from the source, and ultimately interact to help maintain everywhere a generally uniform energy level and spectral shape. The role of internal waves in this view is therefore to spread local, horizontal, non-dissipative motions throughout physical and Fourier space so that the energy can be dissipated or used to mix the ocean vertically.

Is this view true? How much energy does get into the internal wavefield, and how much leaks out? Thorpe (1975), Müller & McComas (1981), and Olbers (1983) summarize some of the more relevant calculations and observations of source and sink strengths. It is striking that almost all the estimates are of order 1 mW m^{-2} or less. For reference, the canonical internal wave spectrum (see the next section) has an energy density per unit surface area of some 3800 J m^{-2}, so a source/sink rate of 1 mW m^{-2} suggests some 44 days as the time taken to fill/drain an internal wavefield completely.

It is tempting to design an internal wave experiment along the lines of the Joint North Sea Wave Project (JONSWAP) (Hasselmann *et al.* 1973), which studied the energy balance of surface waves under conditions of limited fetch. But surface waves clearly have wind as the source, bottom friction (in the JONSWAP case) as the sink, and – compared with internal waves – a relatively constrained dispersion relation and simple geometrical effects. In 1976 at the time of the formation of the scientific plans for JASIN, recent analyses of the Global Atmospheric Research Programme Atlantic Tropical Experiment (GATE) data and some calculations based on weakly nonlinear interactions suggested that we might view depth downward from the surface as a kind of internal wave 'fetch', and thus design an internal wave experiment that looked at successively deeper segments of the water column to see if the vertical asymmetry of the wavefield changed from noticeable near the surface to negligible at depth. Vertical asymmetry implies more energy propagation downwards than upwards, or vice versa, and we could expect that internal waves generated by atmospheric processes would have downward energy propagation. C. H. McComas, who was at Woods Hole at the time, estimated 300 m as the depth above which the internal wave continuum (*cf.* Levine *et al.* this symposium) might show identifiable vertical asymmetry implying downward energy propagation.

We actually designed our measurement array for JASIN to try to do this vertical fetch experiment. Almost all of our instrumentation was above 300 m depth, and our first analyses were of vertical asymmetry in the internal wave continuum. The question initially addressed was: does the spectrum at depth grow because the energy in each frequency band rains down from above, or does near-inertial energy propagate vertically, wave–wave interactions generating the higher frequency energy at each depth? We hoped that by comparing the growth of the spectrum at depth with the vertical energy fluxes in each band we could decide between these alternatives.

What happened can be simply described. The details will not be given. At frequencies higher than inertial and tidal, no consistent pattern could be found during any time period of JASIN or over any depth range in the upper 300 m that clearly showed vertical energy propagation, much less downward propagation following a wind event. To some extent, this null result is due to methodology, because obtaining cross-spectral phases that are significantly different from zero (a necessary condition for vertical asymmetry) requires fairly large asymmetries or considerable statistical confidence. The calculation is briefly described in the next section.

In retrospect, we perhaps tried to address a question with our internal wave experiment in JASIN that was too detailed. Hence the answer is correspondingly vague. Perhaps a broader approach can give more meaningful results.

In this paper, I discuss an examination of the energy content of the internal wavefield, integrated over frequency and depth. Instead of integrating over all frequencies, we examine only those higher than tidal and inertial, for those special bands have much their own dynamics and behaviour. Only horizontal kinetic energy (HKE) is actually calculated, but the assumption of basically linear internal waves lets HKE be unambiguously related to total energy, i.e. horizontal and vertical kinetic energy plus potential energy.

This is an observationalist's approach to internal wave energetics: can we stand back and observe variations in some integral of the internal wavefield that can be related to variations in the levels of source and sink functions? The guiding principle is the radiation balance equation

$$\dot{e} + (\boldsymbol{u} + \boldsymbol{c}_g) \cdot \nabla e = \sum_j s_j, \tag{1}$$

where $e = e(\omega, z)$ is the total energy of the internal wavefield as a function of frequency and depth, $\boldsymbol{u}$ is the horizontal water velocity that may advect internal wave energy into our control volume, $\boldsymbol{c}_g$ is the group velocity (at which energy propagates) at that frequency, and the s_j are source, sink and interaction functions. The s_j might be complicated, even integrals over past time or with other frequencies (i.e. wave–wave interactions).

Note that (1) is just a *description* of how time derivatives, spatial derivatives, and sources and sinks are related; an actual predictive dynamical equation would have to involve various messy things like critical layers, all the wavenumber information, and the inevitable, relentless, nonlinearities. This is meant to be a first look at the variability of the energy of the internal wavefield from a set of observations (JASIN) that is perhaps extensive enough to provide some insights into the energy balances. In effect, we are examining the *envelope* of the internal-wavefield fluctuations and shall compare it with the external environment.

Integration over all frequencies from ω_1 to N, the local buoyancy frequency, yields

$$\dot{\tilde{e}} + (\boldsymbol{u} + \tilde{\boldsymbol{c}}_g) \cdot \nabla \tilde{e} = \sum_j \tilde{s}_j,$$

where $\tilde{e}(z)$ is the total internal wave energy for frequencies higher than ω_1, which will be chosen to be about 0.1 cycles per hour (c/h), that is just higher than tidal. One of the $\tilde{s}_j$ will now represent frequencies lower than ω_1 as being possible sources or sinks for the integrated energy above ω_1. If the winds blow and put energy into near-inertial motions, that energy would change $\tilde{e}$ via the aforementioned $\tilde{s}_j$. The effective group velocity, $\tilde{\boldsymbol{c}}_g$, is defined by

$$\tilde{\boldsymbol{c}}_g \tilde{e} \equiv \int_{\omega_1}^{N} \boldsymbol{c}_g e \, \mathrm{d}\omega.$$

Finally, integration over depth converts $\tilde{e}$ to $\hat{E}$ and the radiation balance becomes

$$\dot{\hat{E}} + (\boldsymbol{U} + \boldsymbol{C}_g) \cdot \nabla_h \hat{E} = \sum_j S_j. \tag{2}$$

Similarly, $\boldsymbol{C}_g$ is defined by

$$\boldsymbol{C}_g \hat{E} \equiv \int_{-D}^{0} \tilde{\boldsymbol{c}}_g \tilde{e} \, \mathrm{d}z, \tag{3}$$

and $\boldsymbol{U}$ is defined similarly from $\boldsymbol{u}(z)$. The S_j include, at least, terms for an energy source/sink in internal wave frequencies lower than ω_1, for the sea surface via wind stress and interacting surface waves, for the entire volume as a source or sink, and for the bottom. The gradients on $\hat{E}$ are strictly horizontal in (2).

Equation (2) will be our phenomenological guide for the analysis of observations. Where (2) is applicable it allows us to relate the time rate of change of the total energy of the high frequency part of the internal wavefield, averaged over depth, to horizontal advection and propagation of larger-scale horizontal gradients of energy and to various source and sink terms at the surface or bottom, or in the volume, or in lower frequency bands.

The likely sources and sinks that we must keep track of are wind stress, horizontal and vertical shear, surface waves, near-inertial waves, and small-scale turbulence and mixing (these being the sinks). Not all of these were observed well in JASIN, and in any case we cannot estimate accurately what fraction of the energy of each process actually passes into or out of internal waves. But at least we can look at the time rate of change of some of the processes and make some inferences.

Some needed initial estimates of spectral levels and group velocities are developed in the next section.

Integrated model spectrum

Munk (1981) described the latest in a series of internal wave models meant to summarize a vertically symmetric, horizontally isotropic, internal-tideless (see Olbers & Pomphrey 1981) wavefield. The basic model has been supported by numerous experiments, and away from special locations (near-surface, extreme topography, equator, hurricanes, etc.) is an excellent first guess at the wavenumber–frequency structure of the internal wavefield (Garrett & Munk 1979).

Munk gives (his § 9.9.1) the spectra and mean-square quantities (integrated over all frequencies in the spectra). At high frequencies, kinetic and potential energy are equal. Integrated over all frequencies, however, Munk's results (and notation) provide

$$\tfrac{1}{2}\langle u^2\rangle/E(z) = \tfrac{3}{4} \tag{4}$$

or, in my notation, integrated horizontal kinetic energy (HKE) is $\frac{3}{4}$ the total energy (E_T). This result assumes the Garrett–Munk spectral slopes of -2; for flatter slopes, as sometimes seen, the HKE is a larger fraction of E_T.

But we are not in this paper going to include the near-inertial and tidal band in our analysis of internal-wavefield fluctuations. Hence we need to relate the high frequency HKE (here denoted E_h) to total energy. The integrals give

$$E_h/E_T \approx \tfrac{3}{4}[1-(2/\pi)\arccos(f/\omega_1)], \tag{5}$$

where $\omega_1 = \alpha f$ and $\alpha = 1.43$ for our JASIN analysis. Thus

$$E_h/E_T = \tfrac{3}{4}\times 0.49 = 0.37. \tag{6}$$

Hence, whatever the total internal wave energy is, we see about 37 % of it in our HKE integrated over frequencies higher than 0.1 c/h.

The total energy derives from the original Garrett & Munk (1972) analysis updated by modest amounts of additional data. From data on the western North Atlantic, Munk (1981) gives the depth-integrated energy as

$$E_T = \int \rho E(z)\,\mathrm{d}z = \rho b^2 E N_0 \int N\,\mathrm{d}z$$

$$\approx \rho b^3 N_0^2 E = 3800\,\mathrm{J\,m^{-2}}, \tag{7}$$

where N_0 and b are scale parameters for the buoyancy frequency distribution $N(z)$, and E is a dimensionlesss scale for the energy content. From the western North Atlantic, (N_0, b, E) are (3 c/h, 1.3 km, 6.3×10^{-5}). Here we write instead, with D as depth,

$$E_T = \rho b^2 E N_0 \bar{N} D = 3800 \text{ J m}^{-2} \tag{8}$$

as actually being the definition (7) of total energy, where $\bar{N}$ is the depth-integrated buoyancy frequency, and let the geographic variation of $\bar{N}$ and D attempt to describe any mean large-scale variation of internal wave energy. The dimensionless scale E takes on the value 5.4×10^{-5} to preserve Munk's western North Atlantic scaling. Note that seasonal variations of $\bar{N}$ due to density changes in only the upper 200 m or so are quite small. We have

$$\bar{N}D = \begin{cases} (0.84 \text{ c/h})\,(5500 \text{ m}) = 8.06 \text{ m s}^{-1} & \text{(Sargasso Sea)} \\ (1.0 \text{ c/h})\,(1500 \text{ m}) = 2.62 \text{ m s}^{-1} & \text{(JASIN).} \end{cases} \tag{9}$$

Hence under this geographical revision of the Garrett-Munk formulation† we expect the JASIN total energy to be smaller than the canonical Garrett–Munk value of 3800 J m^{-2}. In fact,

$$E_T(\text{JASIN}) \approx (2.62/8.06)\, 3800 \text{ J m}^{-2} = 1200 \text{ J m}^{-2}. \tag{10}$$

This value will be used for comparison of observed internal wave energy levels with 'expected' levels; in particular, since $E_h \approx 0.37\, E_T$, the expected 'Garrett–Munk' level of high frequency HKE will be

$$\langle E_h \rangle\,(\text{JASIN}) \approx 450 \text{ J m}^{-2}. \tag{11}$$

We need some additional estimates based on the Munk (1981) spectral description. The horizontal and vertical group velocities are given by $\partial\omega/\partial k$ and $\partial\omega/\partial m$, where k and m are horizontal and vertical (WKBJ) wavenumbers. Using Munk's approximate dispersion relation (not valid near $\omega = N$)

$$m = kN(\omega^2 - f^2)^{-\frac{1}{2}} \tag{12}$$

and noting that

$$k = \pi j b^{-1} \tag{13}$$

relates continuous wavenumbers to discrete mode numbers (j) in the Garrett–Munk formulation, we obtain for $\boldsymbol{C}_g = (C_H, C_V)$

$$C_H = b(\omega^2 - f^2)/2\pi j\omega, \tag{14}$$

$$C_V = b(\omega^2 - f^2)^{\frac{3}{2}}/\pi j\omega N. \tag{15}$$

Scale values for these group velocities are based on choosing $\omega = (\bar{N}f)^{\frac{1}{2}}$, ignoring f with respect to $\bar{N}$, and letting $j = j_* = 3$:

$$\tilde{C}_H \approx b(\bar{N}f - f^2)/2\pi j_*(\bar{N}f)^{\frac{1}{2}} = b(\bar{N}f)^{\frac{1}{2}}/2\pi j_* = 0.032 \text{ m s}^{-1}, \tag{16}$$

$$\tilde{C}_V \approx b(\bar{N}f - f^2)^{\frac{3}{2}}\pi j_*(\bar{N}f)^{\frac{1}{2}}\,\bar{N} = bf/\pi j_* = 0.017 \text{ m s}^{-1} \tag{17}$$

$$= 2(f/\bar{N})^{\frac{1}{2}}\tilde{C}_H = 0.53\,\tilde{C}_H. \tag{18}$$

More important than the group velocities themselves are the energy fluxes formed as the product of group velocity and energy. The Munk (1981) formulation is extended as follows,

† I have looked at the $\bar{N}D$ values for a large set of deep-water locations, ranging from the Mediterranean (*ca.* 1.6 m s^{-1}) to the Arctic (*ca.* 4 m s^{-1}) to the North Pacific (*ca.* 8.9 m s^{-1}), and a few coastal sites (*ca.* 2 m s^{-1}). The coastal sites with shallower water retain a reasonable value for $\bar{N}D$ because the ocean gets shallower from the bottom up, i.e. as D decreases it is the deep, small values of $N(z)$ that are removed from the depth integral.

using F_E where Munk has F_e. In the horizontal, if all the energy is propagating in one direction, the energy flux is

$$\mathscr{F}_H = C_H \rho F_E$$
$$= [\rho b(\omega^2 - f^2)/2\pi j\omega]\,[Eb^2 N_0 NB(\omega)\,H(j)]. \tag{19}$$

The summation over all modes j is

$$\Sigma \mathscr{F}_H = \frac{\rho b^3(\omega^2 - f^2)\,EN_0 NB(\omega)}{2\pi\omega}\left[\frac{\Sigma(j^2 + j_*^2)^{-1} j^{-1}}{\Sigma(j^2 + j_*^2)^{-1}}\right]. \tag{20}$$

For $j_* = 3$ a numerical evaluation of the sums over 100 mode numbers gives $0.187/0.458 = 0.408$ for the term in square brackets. Integrating over all frequencies from f to N gives the total horizontal energy flux:

$$\hat{\mathscr{F}}_H = \int_f^N \sum_j \mathscr{F}_H \,d\omega = \frac{\rho b^3 EN_0(0.41)}{2\pi} \int_f^N \frac{(\omega^2 - f^2)\,B(\omega)\,d\omega}{\omega}$$
$$= \frac{\rho b^3 EN_0 Nf}{\pi^2} \times 1.27. \tag{21}$$

But since $E_T = \rho b^2 EN_0 \bar{N} D$,

$$\hat{\mathscr{F}}_H = \frac{N}{\bar{N}} \frac{b}{D} f \frac{1.27}{\pi^2} E_T$$
$$\approx (1.42 \times 10^{-5})\,E_T = 17\,\mathrm{mW\,m^{-2}} \tag{22}$$

Similarly in the vertical,
$$\mathscr{F}_V = C_V \rho F_E, \tag{23}$$

and the summation over modes and the integration over frequency analogous to (20) and (21) gives

$$\hat{\mathscr{F}}_V = \int_f^N \sum_j \mathscr{F}_V \,d\omega = \frac{\rho b^3 EN_0 Nf}{\pi^2} \times 0.82 \tag{24}$$

$$= \frac{N}{\bar{N}} \frac{b}{D} f \frac{0.82}{\pi^2} E_T = 11\,\mathrm{mW\,m^{-2}}. \tag{25}$$

Since the energy density per unit volume is (again, Munk's scaling)

$$e_T = E_T/b = 0.9\,\mathrm{J\,m^{-3}}, \tag{26}$$

the estimates of integrated effective group velocity from (22) and (25) are

$$\hat{C}_V = \hat{\mathscr{F}}_V/e_T = 0.012\,\mathrm{m\,s^{-1}}, \tag{27}$$

$$\hat{C}_H = \hat{\mathscr{F}}_H/e_T = 0.019\,\mathrm{m\,s^{-1}}. \tag{28}$$

The estimates of effective group velocity here are smaller than the rough values in (16) and (17), but all four values are in the range 1–3 $\mathrm{cm\,s^{-1}}$. The $\hat{C}_H$ estimate will be used later to argue that bodily advection of the internal wavefield by mean currents of 0.01–0.1 $\mathrm{m\,s^{-1}}$ will be at least as important in the energy balance as energy propagation itself, although neither contributes significantly to the energy balance proposed here. The $\hat{C}_V$ estimate will be used to put bounds on the observed vertical fluxes.

The interpretation of these two estimates of integrated energy flux is that if *all* the energy is propagating vertically or horizontally then the fluxes are 11 or 17 $\mathrm{mW\,m^{-2}}$, respectively. In general, the mean energy is mostly partitioned into equal amounts propagating upwards and downwards ('vertical symmetry') and in each direction horizontally ('horizontal isotropy').

The full analysis will not be given here, but suppose we partition Munk's E into $E^{\downarrow}$ and $E^{\uparrow}$ such that

$$E = E^{\downarrow} + E^{\uparrow} \tag{29}$$

$$-\Delta E = E^{\downarrow} - E^{\uparrow} \tag{30}$$

$$= 0 \quad \text{for vertical symmetry.}$$

The coherence γ and phase ϕ between two measurements separated vertically by z will be given by

$$\gamma\, e^{-i\phi} = [E^{\downarrow} \sum_j H(j)\, e^{i\hat{z}j} + E^{\uparrow} \sum_j H(j)\, e^{-i\hat{z}j}]/(E^{\downarrow} + E^{\uparrow}) \sum_j H(j), \tag{31}$$

where the frequency dependence disappears owing to the form of the simplified Garrett–Munk model, and $\hat{z} = \pi b^{-1}(N/N_0)\, z$. Defining $\hat{j}$ by

$$\sum_j H(j)\, e^{\pm i\hat{z}\hat{j}} \equiv e^{\pm i\hat{z}\hat{j}} \sum_j H(j), \tag{32}$$

where $\hat{j}$ is a scale mode number for vertical coherence, we apply Euler's rule to the phase functions in (31) and collect terms to get

$$\gamma \cos\phi = \cos(\hat{z}\hat{j}), \quad \gamma \sin\phi = (\Delta E/E) \sin(\hat{z}\hat{j}), \tag{33}$$

from which $\hat{z}\hat{j}$ can be eliminated to give

$$\Delta E/E = \gamma \sin\phi/(1 - \gamma^2 \cos^2\phi)^{\frac{1}{2}}, \tag{34}$$

relating measured vertical coherence and phase to the vertical asymmetry in the internal wavefield. The result assumes that the upward and downward fields are identical in wavenumber and frequency structure and differ only in their energy level.

Small vertical asymmetries ΔE produce small phases ϕ, which require large coherences and long time series for adequate statistical estimation. For example, at 70 m vertical separation, a coherence of about 0.5 would be typical for internal waves in the mid-frequency range (Desaubies 1976), but $\gamma = 0.5$ requires 100 degrees of freedom to give a phase estimate accurate to 20° (95 % of the time), which by (34) means that $\Delta E/E$ would have to be larger than 0.2, corresponding to an excess of downward (or upward, depending on the sign of the phase) energy of 240 J m^{-2} out of a total of 1200 J m^{-2}, and a net downward (upward) energy flux of 2.2 mW m^{-2}, from (26) and (27). But 100 degrees of freedom at (say) five-hour periods requires 20 days of data, which means that time resolution is lost. In other words, a downward flux of 2 mW m^{-2} for one day following a storm would not be observable in this way. Integrating over frequencies gives more degrees of freedom in shorter records, but these trade-offs are the subject of another paper.

Observations

An overall description of JASIN is available in Pollard (1978; this symposium), and many detailed results of the mooring and meteorological measurements used here are given in Tarbell *et al.* (1979) and Briscoe *et al.* (1979).

The data for internal wave energy came from a subsurface mooring (W1), which carried 23 vector-averaging current meters (VACMS), and a nearby (1.2 km away) surface mooring (W2) which carried 10 vector-measuring current meters (VMCMS). Only the data from instruments at 50, 79, 100, 124, 200, 300, and 1000 m are used for this paper; other analyses (Halpern *et al.* 1981; Weller 1982) have shown both the quality of the data and that sufficient vertical coherence exists for use of all the instruments to be unnecessary. However, if instruments had been available at

depths between 300 and 1000 m and below 1000 m they would have been included for completeness. The layer thicknesses of the water column for which each instrument is used to estimate depth-integrated energy, and the average energy in each layer, are shown in table 1.

The calculations were made by Fourier transforming time series of the east (u) and north (v) current components, setting to zero the coefficients outside the band of interest (here 0.1–4.0 c/h), and retransforming back to a time series. The HKE in the band, is given by $\frac{1}{2}\rho(u^2+v^2)$, and smoothing over the desired interval is done by running-mean filters of specified width, here 72 h. (Figure 1*b* was smoothed by running the filter through twice to compensate for the increased variability from the differencing operation on figure 1*a*.) The filters are centred so that no phase shifts are introduced, but of course data are lost at both ends of the record.

The same general time series of high-frequency HKE came from each depth, once smoothing over several days was applied. There is a slight tendency for the three shallowest records to show the energy pulse around day 220 a little later than do the deeper records (excepting 1000 m), and for the notch between peaks on days 236–238 not to be very evident in the 50 m record.

TABLE 1. CONTRIBUTIONS TO THE DEPTH-INTEGRATED HIGH-FREQUENCY HKE (E_h) FROM THE MEASUREMENTS AT THE SEVEN DEPTHS ANALYSED

(If columns 3 and 5 were identical, each depth layer would be contibuting similarly to the integral.)

instrument depth/m	layer thickness/m	layer thickness (%)	mean E_h in layer / J m^{-2}	E_h in layer (%)
50	65	4	108	14
79	25	2	23	3
100	22	1	15	2
124	50	3	25	3
200	88	6	28	4
300	400	27	100	13
1000	850	57	477	62
totals	1500	100	775	100

Figure 1*a* (solid lines) gives the final depth-integrated, smoothed, high frequency HKE (E_h) for the frequency band 0.1–4.0 c/h. Smoothing over 36 and 72 h is shown for comparison; the 72 hour smoothing will be used henceforth. The canonical Garrett–Munk energy (0.37 E_T, from (6) and (7)) of 1400 J m^{-2} is shown, as well as the depth-scaled estimate (11) of 450 J m^{-2}. The energy E_h fits very nicely between these two limits. If the Garrett–Munk spectrum as a *minimum* expected internal wave energy is a valid concept in the upper ocean, as suggested by Roth *et al.* (1981), perhaps the depth scaling used here lets the concept apply to the depth-integrated energy as well.

Figure 1*b* gives the time-derivative of figure 1*a*, scaled to be presented directly in mW m^{-2}. This quantity, here called $\dot{E}_h$ or energy *rate*, is related to the $\dot{E}$ of equation (2), and it is this time variability that we seek to understand in terms of the sources, sinks, interactions, and advection and propagation. Note that much of the curve resides at values less than $\pm$ 1 mW m^{-2}.

Figure 1*a* (heavy dashed line) shows the near-inertial HKE from the band 0.064–0.078 c/h; the theoretical inertial frequency at 59° N is 0.071 c/h (14 hour period). The plot is also smoothed over three days. See Weller (1982) for a description of the band-passing technique.

Inspection of figure 1*a* indicates that the two major inertial energy peaks *lag* on the corresponding continuum E_h peaks by approximately two days. Also, the inertial energy is everywhere less than the continuum energy.

All the calculations of weakly nonlinear wave–wave resonant interactions (see for example McComas & Bretherton 1977, Olbers 1976) show a transfer of energy from continuum frequencies to near-inertial frequencies; fluxes are some 0.6 mW m^{-2} (Olbers 1982) with the growth rates of the low frequencies taking place in less than 1 to perhaps 100 inertial periods, depending on the vertical scale of the inertial waves.

Writing

$$\dot{E}_\mathrm{i} = E_\mathrm{h}/\tau - E_\mathrm{i}/\tau_\mathrm{ds} \tag{35}$$

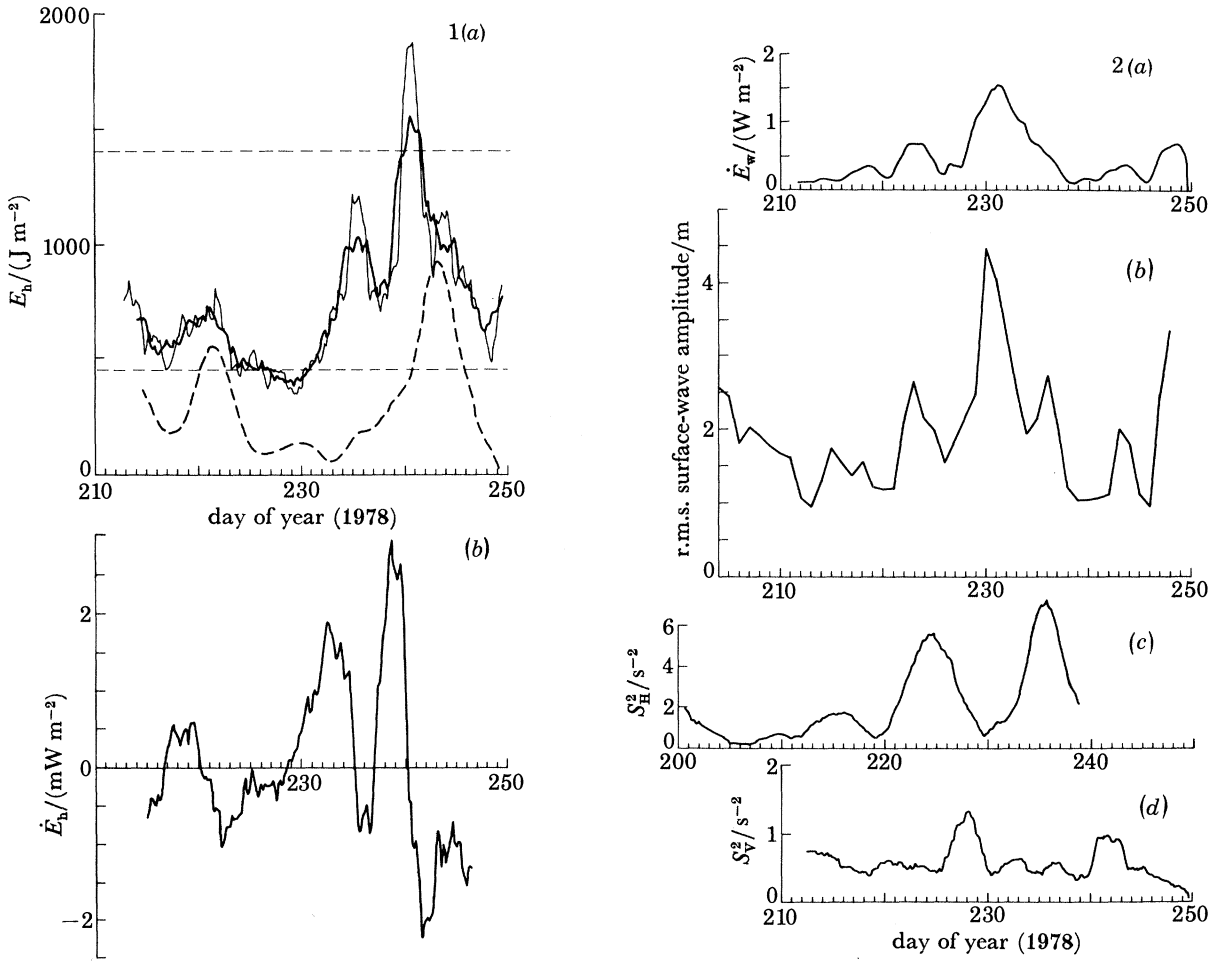

FIGURE 1. Observations of (*a*) internal wave energy against time and (*b*) time rate of change of the high frequency energy. The horizontal axes give the day of the year in 1978; day 230 is 18 August. In (*a*), the solid lines are HKE (E_h) integrated over depth (surface to bottom) and over frequency (0.1–4.0 c/h); the light solid line is smoothed over 36 h, the dark solid line over 72 h. The heavy dashed line is HKE in a band around the local inertial frequency plus or minus 10 %. The horizontal light dashed lines are the Garrett–Munk level (upper line) for this integrated frequency band, and a level (lower line) modified to take into account the local water depth and mean buoyancy frequency (see text). In (*b*), the time-derivative of the dark solid line in (*a*) is given, scaled to be directly in mW m^{-2}. This is $\dot{E}_\mathrm{h}$, the time rate of change of HKE in the internal wave continuum.

FIGURE 2. Possible source functions for internal wave energy: (*a*) the turbulent kinetic energy in the surface wind, calculated by equation (36); (*b*) the r.m.s. surface-wave amplitude (no data were available on day 232); (*c*) the squared horizontal shear (S_H^2) at 200 m depth between moorings I3 and I4; (*d*) the squared vertical shear (S_V^2) between 79 and 300 m depth on mooring W1.

after Olbers (1976) to relate growth of inertial energy $\dot{E}_i$ at 0.4 mW m^{-2} to the continuum energy as a source, and allowing the E_i to dissipate at some rate τ_{ds}^{-1}, which is presumably faster than the rate τ^{-1} at which the inertial band gains energy, we can roughly fit the curves of figure 1*a* together by letting $\tau = 10$ days, and $\tau_{ds} = 2.5$ days. Then, for example, the growth of the inertial peak on day 221 in figure 1*a* is due to the energy in the continuum on day 219. In four days at 0.4 mW m^{-2}, 140 J m^{-2} have been transferred (net) to the near-inertial band out of the continuum, which accounts for the decay of the continuum peak back to the scaled Garrett–Munk value.

During the same four days, energy is dissipated out of the inertial band at a slower rate, perhaps (τ_{ds}/τ) 0.4 mW m^{-2} = 0.1 mW m^{-2}. This lost energy presumably goes partly into mixing and is partly lost into turbulent dissipation.

This explanation is a tempting way to combine the curves in figure 1*a*, but fails to account for the peak in E_h on the middle day 234. It is frankly discomforting in an air–sea interaction experiment to say that the inertial oscillations were generated by the internal waves, rather than vice-versa, but these are deep inertial oscillations and so at least do not contradict the near-surface results of Weller (1982).

Figure 1 is based on direct observations from moorings W1 and W2 and is the principal result of this paper. Figure 2 displays several possible source functions, and figure 3 speculates on how to combine the source functions to arrive at the observations in figure 1.

Figure 2*a* illustrates the total kinetic energy flux in the atmospheric boundary layer, over all frequencies, calculated in the time domain as

$$\dot{E}_W = \rho_A C_D U_A^3, \tag{36}$$

where ρ_A is air density (1.25 kg m^{-3}), C_D is a drag coefficient (1.3×10^{-3} is used), and U_A is wind speed at the anemometer on buoy W2 (Briscoe *et al.* 1979). The three-day smoothing used in the plot smears out the details of the major JASIN wind event of up to 17 m s^{-1} (thus about 0.5 Pa) during days 229–233 (17–21 August), in which more than 2000 mW m^{-2} were in the atmospheric boundary layer.

Oakey & Elliott (1982) have shown how small-scale dissipation in the mixed layer is nicely described as about 1 % of the wind energy flux. The relation seems to hold for the JASIN data as well (Oakey 1982 personal communication). Therefore 1 % of $\dot{E}_W$ of figure 2*a* may be an estimate of upper-ocean dissipation during JASIN, suggesting maximum values of 30 mW m^{-2} on day 231, while most participants were in Glasgow between cruises, and some 10 mW m^{-2} toward the end of the record.

Denman & Miyake (1973) observed that about 0.12 % of the turbulent kinetic energy flux in the wind appeared as a potential energy increase in the mixed layer, owing to mixed-layer deepening. This suggests that 1–4 mW m^{-2} were available in JASIN for mixed-layer deepening.

In addition to mixing the upper ocean, the wind makes surface waves and causes inertial motions, both of which are possible sources of internal waves, and the wind can also generate higher-frequency internal waves directly. Olbers & Herterich (1979) and Olbers (1983) estimate 1 mW m^{-2} as an upper bound for internal wave generation (low modes at high frequencies) from a pair of surface waves, using realistic mixed-layer thickness and depth, large buoyancy frequencies, realistic wave spectra, and a surface-wave variance of 2 m^2. Figure 2*b* shows the daily-averaged significant wave height (Dobson 1980) for the JASIN area; the r.m.s. wave displacement is $\frac{1}{4}$ these values. The surface waves sharply peaked on day 231 at about 1.3 m^2, and were even larger, but were unmeasured, on day 232. By being generous and accepting 1 mW m^{-2}

from surface waves near day 231, it is just possible to account for half of the growth rate $\dot{E}_h$ in figure 1*b* during days 231–234.

During days 231–234, we observed that the strong winds were blowing to the north on day 231, and slowly shifted to east by day 234. According to the Olbers & Herterich calculations, one expects in the seasonal thermocline high-frequency low-mode internal waves travelling normal to the surface waves, and hence normal to the wind. East–west high frequency internal waves would show up as an anisotropy in the current meter records.

Day 232 does show an energy increase in the 1.0–2.5 c/h band at 100 and 124 m depths (but *not* at 79 m), and some hints of anisotropy, but the result is quite weak. The data on hand, as currently analysed, are perhaps consistent with, but do not prove, a generous interpretation of the Olbers & Herterich (1979) model calculations.

Figure 2 also presents the time-varying horizontal (*c*) and vertical (*d*) shears. The horizontal shear comes from the I3 and I4 moorings at 200 m depth; I3 and I4 are some distance from W1 and W2, a problem discussed in the next paragraph. The quantity displayed is

$$S_H^2 = \left(\frac{\partial u}{\partial y}\right)^2 + \left(\frac{\partial v}{\partial x}\right)^2, \tag{37}$$

where u and v are east and north components of current, and x and y point east and north. Brown & Owens (1981) validate the concept of horizontal shear working on an horizontal effective viscosity as a way to get energy out of the large-scale flow and into internal waves, as first proposed by Müller (1976). The horizontal viscosity obtained in Brown & Owens for the continuum part of the internal wave band was

$$\nu_h = 200\,\mathrm{m^2\,s^{-1}}, \tag{38}$$

which multiplied by (37) gives an energy dissipation rate from the eddies, i.e. the source of the horizontal shear. Estimating 800 m (Pennington & Briscoe 1979) as the thickness d of the eddy structures providing the shear in JASIN, and using $\tilde{\nu}_h = \frac{1}{3}\nu_h$ since our internal wavefield is about one third as energetic as that of Brown & Owens, we have

$$\dot{E}_{SH} = \rho S_H^2 \tilde{\nu}_h d = 2.7\,\mathrm{mW\,m^{-2}}. \tag{39}$$

Unfortunately, the horizontal shear and inferred energy flux in figure 2*c* cannot be unambiguously related to the rate of change $\dot{E}_h$ in figure 1*b* because the shear is estimated between moorings I3 and I4 some 40 km to the southeast of W1 and W2 where the internal wave energy was measured. Brown & Owens (1981) show time series of mean squared horizontal and vertical shear, but there is no close correspondence in time between peaks in the two series, which is not surprising for baroclinic eddies; this means we cannot use vertical shear from W1 to estimate a 'time-shift' for the I3–I4 horizontal shear.

Our observation of vertical shear (squared) is nevertheless given in figure 2*d*. It is calculated from the instruments at 79 and 300 m (depth) on W1. Since no significant energy transfer to the internal wavefield is caused by the vertical shear (Ruddick & Joyce 1979, Brown & Owens 1981), and since we cannot deduce horizontal shear from vertical shear, it will not be discussed further. It is shown only to give the magnitudes, which for both horizontal and vertical shear (squared) compare with those of Brown & Owens.

The analyses of JASIN hydrography (see for example Pollard 1982) suggest the eddy structures moved west to northwest at about 2 km day^{-1} during JASIN. The centre point of the I3–I4 pair is some 18–42 km away from W1, depending on whether one measures distance west or northwest.

Hence delays of 9–21 days are expected before any horizontal shears between I3 and I4 appear at W1, assuming little evolution of the eddy field.

If S_H^2 in figure 2*c* is shifted 9–21 days later and compared with figure 1*b*, we see that a shift of of 14 days puts the first large S_H^2 peak (actually on day 224) on day 238 right on top of the large positive peak in $\dot{E}_h$ (figure 1*b*) that gives rise three days later to the 1500 J m^{-2} peak on day 231 in figure 1*a*.

Having time-shifted S_H^2 (note that no other shift of between 9 and 21 days provides as much overall correspondence), we see that the largest shear peak (days 235–236 actual, 249–250 shifted) runs off the end of our observational record of internal waves. The amplitude of the inferred energy flux on day 238 from (39) is 2.7 mW m^{-2}, compared with the observed $\dot{E}_h$ of about 2.5 mW m^{-2}.

The second term in (2) must be considered. If there are horizontal gradients in the depth-integrated energy then advection or propagation could change E_h at our observational site. Since figure 1*a* shows differences of 1000 J m^{-2} in E_h are possible at different times at our one site, it seems possible that differences of 1000 J m^{-2} could occur between two sites at one time. The distance between the different sites is estimated as at least 10 km, which corresponds to frontal zone widths and the distance an eddy edge might move in five days. Therefore

$$\begin{aligned} \dot{E}_A &= (0.01\,\mathrm{m\,s^{-1}})\,(1000\,\mathrm{J\,m^{-2}})/10\,\mathrm{km} \\ &= 1\,\mathrm{mW\,m^{-2}} \end{aligned} \tag{40}$$

is an estimate of the largest advective/propagative flux we might expect, per 0.01 m s^{-1} velocity increment.

In general, the mean flow velocities are normal to the major horizontal gradients of eddy properties. Even if eddies are pumping up internal waves in some regions and not in others, the rate at which those regions advect is small (perhaps 0.02 m s^{-1}) and the gradients along the advection direction are also small. Let an eddy advect at speed V for time T, while pushing $\dot{E}$ mW m^{-2} into the internal wavefield over a region $R = VT$; then the advective flux is at most

$$V\dot{E}T/VT = \dot{E} \tag{41}$$

and is overestimated because propagation away from the generation region has not been included. The propagation occurs at the group velocity (28) but tends to go in all directions from the source region, which causes the source level to decay but does not add especially to the advective flux seen at a particular point.

An advective flux from an internal wave 'hot spot' that exists independently of the eddy field could be large, for then the mean flow might be parallel to the energy gradients. Such a hot spot could come from a local wind event, for example.

Actual net horizontal propagation of internal wave energy for a non-isotropic spectrum is also small. An examination of the eastward E_h against the northward E_h gives fluctuations of some $\pm$ 50 J m^{-2}, or about $\pm$ 10 % of the scaled Garrett–Munk level. At an effective group velocity of 0.02 m s^{-1}, this corresponds to a net horizontal flux of perhaps 0.7 mW m^{-2} at most.

One curious anisotropy does occur on day 236, precisely at the time the strong negative flux occurs in figure 1*b*. The depth-integrated, high frequency averaged Reynolds stress $\langle uv \rangle$ swings sharply negative for just over one day, whereas it is positive for all other times between days 221 and 247 except for a brief period on 240 when it is weakly negative. The measurements from

moored current meters (Tarbell *et al.* 1979) show a one-day appearance of anomalously cold water at W1 on day 236, which is coincident with the negative Reynolds stress and negative E_h. I cannot construct a coherent picture of this incident.

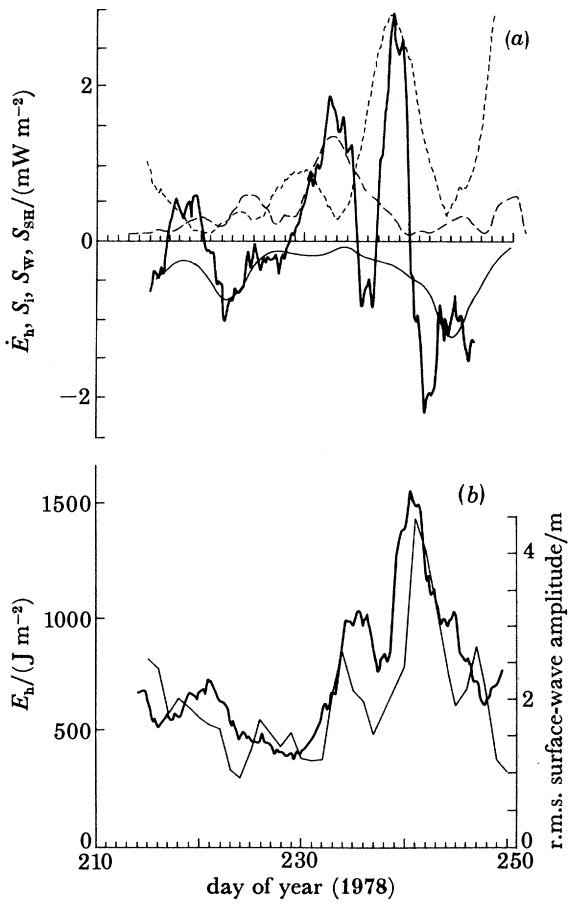

FIGURE 3. (*a*) Speculative energy balance and (*b*) correspondence between surface-wave amplitude, delayed by eleven days, (light line and right axis) and E_h (dark line and left axis). The four curves in (*a*) are $\dot{E}_h$ from figure 1 *b* (dark solid), inertial energy from figure 1 *a*, S_i (light solid), wind energy from figure 2 *a*, S_W (heavy dashed), and horizontal shear from figure 2 *c*, S_{SH} (light dashed). See text for scaling and time shifts.

Summarizing these observations, we have the following:

(i) a time-varying E_h (figure 1 *a*), which corresponds to three positive $\dot{E}_h$ periods (figure 1 *b*) alternating with three negative $\dot{E}_h$ periods;

(ii) two periods of strong near-inertial energy (figure 1 *a*), which correspond in time to the first and third negative $\dot{E}_h$ periods;

(iii) one period of strong wind energy flux (figure 2 *a*), which corresponds after a 36 hour lag to the second positive $\dot{E}_h$ period;

(iv) one period of strong squared horizontal shear (figure 2 *c*), shifted 14 days later to allow for the relative position of moorings, which corresponds to the third positive $\dot{E}_h$ period;

(v) an unexplained period of negative $\dot{E}_h$ (the second negative period) that coincides with an arrival at the mooring of a pulse of cold water and a change in sign of the mean value of $\langle uv \rangle$.

Energy balance

Here I attempt to combine the preceding information into a speculative energy balance; to be more definitive would require measured horizontal gradients of internal wave energy, measured horizontal shears at the site of internal wave measurements, and considerable calculation effort on both wind and surface waves as source functions.

Figure 3*a* gives the balance suggested by the observations and the analysis in the preceding section. The first positive $\dot{E}_h$ peak is small and unexplained except that it closely follows a peak in squared horizontal shear, the third positive $\dot{E}_h$ peak comes from the horizontal shear (time-shifted 14 days); the second positive $\dot{E}_h$ peak comes from the wind, with a lag of 36 hours, suggesting surface-wave interactions as a possible mechanism because time would be needed for the surface variance to grow; the first and third negative $\dot{E}_h$ peaks come from the transfers out of the continuum into near-inertial motions, with a lag of one day; and the second negative $\dot{E}_h$ peak is unexplained except for its coincidence with peculiar hydrographic behaviour on that day, suggestive in fact of the passage of a sharp frontal feature between two water masses.

There is no major contradiction from the near-inertial waves draining energy out of the continuum internal waves for the first and third energy peaks in figure 1*a* but not for the second peak. If the first and third peaks do arise from an energy flux from the horizontal shear working on an effective horizontal viscosity, then the energy entering the continuum does so at high frequencies in the volume, hence around $\bar{N}$ (Müller 1977), whereas the energy flux from surface waves appears at high frequencies in the seasonal thermocline, hence around the maximum N in the water column (Olbers & Herterich 1979). The parametric subharmonic instability (PSI) that transfers energy from the continuum down into near-inertial frequencies does so from intermediate frequencies in the water column, so would be more efficient from the horizontal shear-generated internal waves.

Also, the near-inertial motions that are apparently generated by this PSI mechanism are in the volume, not near the surface, presumably because the horizontal shears are larger at depth. Previous searches for wind-generated inertial motions have been successful near the surface but have been confounded at depth by incoherent, even upward-propagating (energy) motions; perhaps PSI is their source, as suggested by Olbers (1976).

Figure 3*a* shows

$$\dot{E}_h + (\boldsymbol{U} + \boldsymbol{C}_g) \cdot \nabla_h E_h = S_{SH} + S_W + S_i, \tag{42}$$

where the advective term on the left-hand side is ignored except for its possible role in the notch between days 236 and 238 in figure 1*a*. From (39) we have

$$S_{SH} = \rho \tilde{\nu}_h d \left[\left(\frac{\partial u}{\partial y} \right)^2 + \left(\frac{\partial v}{\partial x} \right)^2 \right], \tag{43}$$

with $\tilde{\nu}_h = 200/3\ \mathrm{m^2\,s^{-1}}$ and $d = 800\ \mathrm{m}$;

$$S_W = 4.5 \times 10^{-4} \rho_A C_D U_A^3 \tag{44}$$

and hence about 0.05 % of the wind flux gets into the internal wave continuum, with a lag of 36 hours;

$$S_i = -E_i/\tau_i, \quad \tau_i = 7.8 \times 10^5\ \mathrm{s} = 9\ \mathrm{days}, \tag{45}$$

with a lag of one day. The transfer time τ_i is surprisingly close to the earlier estimates based on (35).

Note that Denman & Miyake (1973) found that about 0.12 % of the wind flux went into mixed-layer deepening; here we find about 0.05 % going into internal waves. This is consistent with the suggestion of Linden (1975) that radiation of internal waves may decrease the energy available for mixed-layer deepening.

Dissipation has been ignored here based on estimates from Oakey (1982) and others (Desaubies & Smith 1982) of its smallness (away from the mixed layer) relative to these depth-integrated fluxes of order 1 mW m^{-2}.

Figure 3*a* is, of course, a terrible energy balance in detail. Nothing fits very well, there is a lot of arbitrariness in the horizontal shear time-shifting, physics are missing from the wind-input source term, and 35–40 days is much too short a time scale on which to look at eddy-scale shears and do any quantitative correlations. Nevertheless, the fact that the fit is as good as it is and that the *magnitudes* of the source terms are reasonable is encouraging, even exciting. There is hope for this approach.

Figure 3*b* presents a surprising correspondence between the figure 1*a* E_h and the figure 2*b* surface-wave r.m.s. amplitude; the latter is delayed eleven days for plotting. Figure 2*b* could also have been overplotted on figure 1*b*, for $\dot{E}_h$, in which case the waves would have been delayed only eight days for the best correspondence in the plot.

The energy in the surface wavefield varies from 300 to 6400 J m^{-2} (0.25 to 1.1 m r.m.s. wave amplitude). Relating the 6400 J m^{-2} surface-wave peak to the 2.6 mW m^{-2} maximum rate of change of E_h suggests a transfer time scale of 27 days, rather long compared with the rates of the other possible source processes. Olbers & Herterich (1979) wrestled with this slow rate as well and concluded that surface-wave generation of internal waves was probably important only for waves in the seasonal thermocline, not for the whole water column. If the correspondence in figure 3*b* is not an accident, this conclusion may need re-examination.

Conclusions

In this analysis of data from an air–sea interaction experiment, from which we expected to see high frequency internal waves being energized at depth by energy propagated there as near-inertial waves that were generated elsewhere by the wind stress, we have observed instead a tenuous but fascinating balance between generation by horizontal shear and wind (possibly via surface waves), and losses to near-inertial motions by resonant interactions.

It is likely that we lost sensitivity to direct air–sea interaction generation by the artifice of depth and frequency integration. Relaxation of the depth integral, and attention to the short period of high winds in the record, might yet allow further study of wind-generated internal waves.

Confirmation is needed that the deep inertial motions are being generated locally by PSI resonant interactions, rather than just being propagated from elsewhere. Some elements of this question may be addressable by the larger-scale, long-term JASIN array, but this is another study entirely.

The magnitude of fluxes and estimated transfer times seen here indicate that the question offered in figure 1 of Gregg & Briscoe (1979) should be resolved in favour of their lower left picture: little energy passes through the internal wavefield, so little vertical mixing is driven by it. The importance of the internal wavefield in an overall energy balance is apparently as a sink for eddy energy (see Woods 1980).

My thanks to Raymond Pollard and Henry Charnock, F.R.S., for encouraging me eight years ago to participate in JASIN, and for their continued interest and enthusiasm since. The JASIN style of a closely knit but informal organization that depends on the scientific motivation and quality of the participants was exciting to partake of and contribute to, and exhausting at times.

The work described here owes its genesis to many discussions with Hank McComas, its performance to numerous scientific and technical colleagues in the Buoy Group at Woods Hole and in other laboratories, and its analysis to considerable effort by Nancy Pennington and especially Bob Weller. Helpful conversations, both pro and con, with Weller, Terry Joyce, Nick Fofonoff, Breck Owens, and Dirk Olbers are acknowledged. Data and figures from Weller and John Gould were gratefully received.

Financial support over the years has come from the National Science Foundation under grant OCE77-25803, and especially from the Office of Naval Research under contract N00014-76-C-0197; NR 083-400. This is WHOI contribution no. 5180.

References

Bell, Jr., T. H. 1975 Topographically generated internal waves in the open ocean. *J. geophys. Res.* **80**, 320–327.

Bell, Jr., T. H. 1978 Radiation damping of inertial oscillations in the upper ocean. *J. Fluid Mech.* **88**, 289–308.

Briscoe, M. G., Mills, C. A., Payne, R. E. & Peal, K. R. 1979 *Atlantis*-II (cruise 102) moored and shipboard surface meteorological measurements during JASIN 1978. Technical report WHOI-79-43, Woods Hole Oceanographic Institution, Massachusetts, U.S.A. (80 pp.).

Brown, E. D. & Owens, W. B. 1981 Observations of the horizontal interactions between the internal wavefield and the mesoscale field. *J. phys. Oceanogr.* **11**, 1474–1480.

Denman, K. L. & Miyake, M. 1973 Upper layer modification at Ocean Station *Papa*: observations and simulation. *J. phys. Oceanogr.* **3**, 185–196.

Desaubies, Y. J. F. 1976 Analytical representation of internal wave spectra. *J. phys. Oceanogr.* **6**, 976–981.

Desaubies, Y. J. F. & Smith, W. K. 1982 Statistics of Richardson number and of instability in oceanic internal waves. *J. phys. Oceanogr.* **12.** (In the press.)

Dobson, F. W. 1980 Surface waves. JASIN news, no. 20, pp. 2–4, 15–16.

Fu, L.-L. 1981 Observations and models of inertial waves in the deep ocean. *Rev. Geophys. Space Phys.* **19**, 141–170.

Garrett, C. 1979 Mixing in the ocean interior. *Dyn. Atmos. Oceans* **3**, 239–265.

Garrett, C. J. R. & Munk, W. H. 1972 Space–time scales of internal waves. *Geophys. Fluid Dyn.* **2**, 225–264.

Garrett, C. & Munk, W. H. 1979 Internal waves in the ocean. *A. Rev. Fluid Mech.* **11**, 339–369.

Gregg, M. C. & Briscoe, M. G. 1979 Internal waves, finestructure, microstructure and mixing in the ocean. *Rev. Geophys. Space Phys.* **17**, 1524–1548.

Halpern, D., Weller, R. A., Briscoe, M. G., Davis, R. E. & McCullough, J. R. 1981 Intercomparison tests of moored current measurements in the upper ocean. *J. geophys. Res.* **86**, 419–428.

Hasselmann, K., Barnett, T. P., Bouws, E., Carlson, H., Cartwright, D. E., Enke, K., Ewing, J. A., Gienapp, H., Hasselmann, D. E., Kruseman, P., Meerburg, A., Müller, P., Olbers, D. J., Richter, K., Sell, W. & Walden, H. 1973 Measurements of wind–wave growth and swell decay during the Joint North Sea Wave Project (JONSWAP). Reihe A (8°), no. 12, Deutches Hydrographisches Institut, Hamburg, F.R.G. (95 pp.).

Käse, R. H. 1979 Calculations of the energy transfer by the wind to near-inertial internal waves. *Deep-Sea Res.* **26**, 227–232.

Käse, R. H. & Olbers, D. J. 1979 Wind-driven inertial waves observed during phase III of GATE. *Deep-Sea Res.* Supp. to **26**, 191–216.

Leaman, K. D. 1976 Observations on the vertical polarization and energy flux of near-inertial waves. *J. phys. Oceanogr.* **6**, 894–908.

Linden, P. F. 1975 The deepening of a mixed layer in a stratified fluid. *J. Fluid Mech.* **71**, 385–405.

McComas, III, C. H. & Bretherton, F. P. 1977 Resonant interaction of oceanic internal waves. *J. geophys. Res.* **82**, 1397–1412.

McComas, III, C. H. & Müller, P. 1981 The dynamic balance of internal waves. *J. phys. oceanogr.* **11**, 970–986.

Müller, P. 1976 On the diffusion of momentum and mass by internal gravity waves. *J. Fluid Mech.* **77**, 789–823.

Müller, P. 1977 Spectral features of the energy transfer between internal waves and a larger-scale shear flow. *Dyn. Atmos. Oceans* **2**, 49–77.

Müller, P. & McComas, C. H. 1981 Dynamics and energy balance of oceanic internal waves. In *Nonlinear properties of internal waves*, (ed. B. J. West), American Institute of Physics conference proceedings no. 76, pp. 181–201.

Müller, P., Olbers, D. J. & Willebrand, J. 1978 The IWEX spectrum. *J. geophys. Res.* **83**, 479–500.
Munk, W. 1981 Internal waves and small-scale processes. In *Evolution of physical oceanography* (ed. B. A. Warren and C. Wunsch), pp. 264–291. Cambridge, Massachusetts: MIT Press.
Oakey, N. S. 1982 Determination of the rate of dissipation of turbulent energy from simultaneous temperature and velocity shear microstructure measurements. *J. phys. Oceanogr.* **12**, 256–271.
Oakey, N. S. & Elliott, J. A. 1982 Dissipation within the surface mixed layer. *J. phys. Oceanogr.* **12**, 171–185.
Olbers, D. J. 1976 Nonlinear energy transfer and the energy balance of the internal wave field in the deep ocean. *J. Fluid Mech.* **74**, 375–399.
Olbers, D. J. 1983 Models of the oceanic internal wavefield. *Rev. Geophys. Space Phys.* (In the press.)
Olbers, D. J. & Herterich, K. 1979 The spectral energy transfer from surface waves to internal waves in the ocean. *J. Fluid Mech.* **92**, 349–379.
Olbers, D. J. & Pomphrey, N. 1981 Disqualifying two candidates for the energy balance of oceanic internal waves. *J. phys. Oceanogr.* **11**, 1423–1425.
Pennington, N. & Briscoe, M. G. 1979 *Atlantis*-II (cruise 102) preliminary CTD data from JASIN 1978. Technical report WHOI-79-42, Woods Hole Oceanographic Institution, Massachusetts, U.S.A. (225 pp.).
Pollard, R. T. 1978 The Joint Air–Sea Interaction experiment – JASIN 1978. *Bull. Am. Soc.* **59**, 1310–1318.
Pollard, R. T. 1982 Mesoscale (50–100 km) circulations revealed by inverse and classical analysis of the JASIN hydrographic data. *J. phys. Oceanogr.* (In the press.)
Roth, M. W., Briscoe, M. G. & McComas, III, C. H. 1981 Internal waves in the upper ocean. *J. phys. Oceanogr.* **11**, 1234–1247.
Ruddick, B. 1980 Critical layers and the Garrett–Munk spectrum. *J. mar. Res.* **38**, 135–145.
Ruddick, B. R. & Joyce, T. M. 1979 Observations of interaction between the internal wavefield and low-frequency flows in the North Atlantic. *J. phys. Oceanogr.* **9**, 498–517.
Tarbell, S., Briscoe, M. G. & Weller, R. A. 1979 A compilation of moored current meter and wind recorder data, volume VXIII (JASIN 1978, moorings 651–653). Technical report WHOI-79-65, Woods Hole Oceanographic Institution, Massachusetts, U.S.A. (233 pp.).
Thorpe, S. A. 1975 The excitation, dissipation, and interaction of internal waves in the deep ocean. *J. geophys. Res.* **80**, 328–338.
Weller, R. 1982 The relation of near-inertial motions observed in the mixed layer during the JASIN (1978) experiment to the local wind stress and to the quasigeostrophic flow field. *J. phys. Oceanogr.* **12**, 1122–1136.
Woods, J. D. 1980 Do waves limit turbulent diffusion in the ocean? *Nature, Lond.* **288**, 219–224.

Discussion

R. T. POLLARD (*Institute of Oceanographic Sciences, Brook Road, Wormley, Godalming, Surrey GU8 5UB, U.K.*).

(1) Can Taylor's hypothesis be invoked to obtain shear estimates at the Fixed Intensive Array rather than 40 km off at I3 and I4?

(2) Is the eddy scale the correct one to choose for horizontal shear estimates, or would a shorter frontal scale be more appropriate?

(3) Dr Briscoe suggests that energy from the continuum flows into inertial motions. How is that energy lost?

M. G. BRISCOE

(1) This has been attempted, but the quality of the answer is uncertain. The I3–I4 horizontal shear estimate used here assumes a non-evolving eddy field, but is not contaminated by vertical shears. The horizontal shear estimated by using Taylor's hypothesis on W1 currents also assumes a frozen field, but is contaminated by vertical shear. The approach has merit, perhaps, but its value has not yet been studied.

(2) The original Müller analysis uses a WKBJ assumption for the mean-shear and internal wavefield scales; a 10 km or shorter frontal scale is close to violating this assumption. The frontal region would perhaps be implicit in a Taylor-hypothesis shear estimate (previous question) anyway.

(3) I don't know. Conventional wisdom would require that it go to vertical mixing and